RESEARCH

Hybrid modelling and analysis of cutter suction dredger using hardware and software in the loop

C. R. Barik[1] · K. Vijayan[1] · O. P. Sha[1] · K. Shrivastava[1]

Abstract

The current study identifies the critical design considerations for the universal joint of a cutter suction dredger. The cutter suction dredger is modelled as a hybrid two subsystems consisting of hardware-in-the-loop (HIL) and Software-in-the-loop (SIL). HIL, consisting of Dredge hull, spud and soil embedment, is modelled experimentally. System identification is carried out, and a single degree of freedom (SDOF) system is determined for HIL. The identified dynamic parameters are interfaced with the SIL. SIL consisting of the cutter shaft is modelled numerically. The primary and secondary shaft of the cutter shaft is coupled using springs to emulate the universal joint. A sensitivity analysis of the acceleration amplification based on the spud location relative to the hull is carried out. It is observed that the spud position relative to the hull has less influence on the acceleration amplification. A soft universal joint produces a higher response transmitted to the Dredge hull. Further, the influence of the universal joint on the fatigue life of the shaft is analyzed. The results from the fatigue analysis indicate that higher coupling stiffness reduces the fatigue life of the cutter shaft. Therefore, while designing the universal joint, both the impulsive and the fatigue loading must be considered.

1 Introduction

In recent years there has been an increased demand for dredging due to the requirement for the development of coastal shipping inland waterways in India. Dredging removes sediments and debris from the bottom of lakes, rivers, harbours, and other water bodies. Deepening channels and waterways increases channel flow capacity and allows larger vessels to navigate safely. It is a routine necessity in waterways because sedimentation gradually fills the channels and harbours. Therefore, there is an increased demand for understanding the response of a dredger to operate it efficiently with reduced downtime. In the current study, a cutter suction dredger (CSD) is considered, used in India for various operations such as beach reclamation works in Puducherry and the development of national waterways. A typical schematic of a cutter suction dredger is shown in Fig. 1.

Previously researchers have developed an experimental prototype of scale 1:6 for the CSD at Texas A&M University to measure the cutting force using the dredge/tow carriage. The flume was equipped with a sediment pit measuring with an observation well where the sediment pit can be viewed when a test is in progress. A carriage was positioned on top of two guide rails (at the top of the dredge/tow flume) (Glover 2002; Glover and Randall 2004; Randall et al. 2005; Young 2009). Koning et al. (1983) focused on the effect of wave loading to predict the dynamic behaviour of the cutter head. The predicted theory indicated that low swing velocities and high cutter revolutions could reduce the load on the cutter head. It showed that the surge force, the heave force and the cutter torque were increased by the oscillating movement of the cutter head in the heave direction. The interaction of the dredge hull with the spud is similar to other offshore structures, such as spar platforms (Soeb et al. 2017) and offshore wind turbines (Sclavounos et al. 2019), which are moored or anchored to the soil. Soeb et al. (2017) analyzed a moored Spar hull using ABAQUS/AQUA for surge, heave, and pitch response. Mooring tensions variation with water depth and load for different sea state conditions was investigated. It has been observed that the platform response decreases due to

✉ K. Vijayan
  kiran.vijayan@naval.iitkgp.ac.in

1 Department of Ocean Engineering and Naval Architecture, IIT Kharagpur, Kharagpur, India

Fig. 1 Schematic overview of the cutter suction dredger
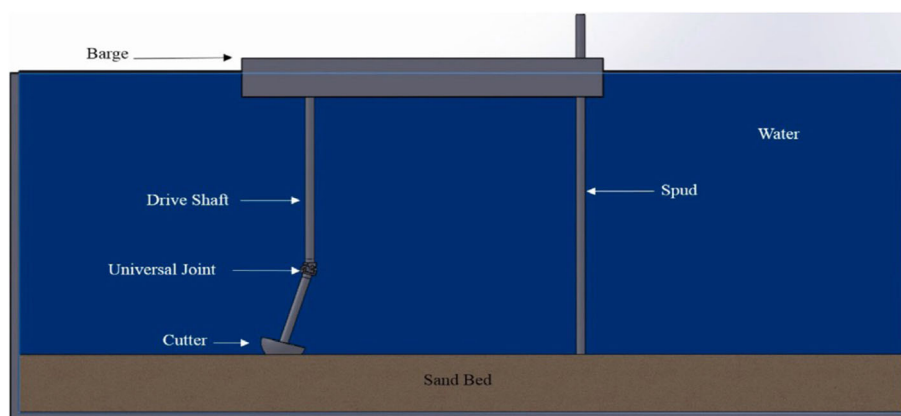
increased damping of mooring lines, and the current reduces the dynamic fluctuation.

Wave loading on the offshore cylindrical structures which has diameter to wavelength ratio less than 0.05 can be estimated using Morison's equation. Various authors have numerically estimated the wave forces on slender structures (Wolfram and Naghipour 1999; Arena and Nava 2008) using the Morison equation. The response of offshore structures could be nonlinear due to the material (Jameel et al. 2017) or the forcing conditions (Mockutè et al. 2017). Najafian et al. (2000) carried out an experimental study on a flexible cylinder subjected to wave loading. The nonlinearity in the Morison force on a flexible structure was mainly due to the nonlinear drag force. Various authors (Stansberg 1997; Chaplin et al. 1997; Wolfram 1999) have attempted to develop an equivalent linear model of the system using techniques such as statistical linearization.

The forces and torque generated during excavation are critical for dredger operation. For calculating these forces and torques, it is essential to know the characteristics of the sea bed surface (like sand, clay and rock) where the dredging operation is carried out. Adequate cutting theories are required to determine the forces required for the excavation (van Os and van Leussen 1987; Miedema 1992, 2009; Yasheng et al. 2006; Helmons and Miedema 2013; Chen et al. 2014, 2015; Helmons et al. 2014). During the mid-80 s, Miedema (1986) carried out experiments to validate the cutting theory models using compacted sand of high and low density with and without considering the inertial forces, water resistance and gravitational force. The results from experiments indicated that the cutting force model was a function of underwater pressure, cutting forces and shear angles. Miedema (1989) derived the expression for forces and torques appearing on the excavating elements. With some basic assumptions, such as the cutter head is conical and the blades have an angle with the cutter head axis, the cutting force on the straight blade was determined by considering

the cutting theory of water-saturated sand, which applies to the cutter head.

The random forces from the water environment and the cutting action can generate random stresses on the structure leading to fatigue damage. Several researchers (Yigang et al. 1993; Amzallag et al. 1994; Lagoda 1996; Ariduru 2004; Baek et al. 2008; Shen et al. 2010; Marsh et al. 2016; Salvinder et al. 2016) have developed methods to characterize the fatigue damage of the structure. Rédl (2018) analyzed fatigue using the rainflow counting method on the experimental stress obtained during agricultural ploughing. Prasad and Sekhar (2018) experimented on a rotating shaft to analyze fatigue life using both the time and frequency domain approaches. The fatigue life was estimated using the time domain approach using the rainflow count method and Palmgren–Miner rule and the frequency domain approach using narrow-band approximation and Dirlik's empirical solution.

The maintenance of the required depth in the meandering and braided waterway requires the complex operation of the cutter suction dredger. Based on the literature, modelling and analysis of such a complex structure as CSD can be carried out using a hybrid approach. For numerical simulation using the hybrid approach, the substructuring technique (Wagg and Stoten 2001; Plummer 2006; Bursi and David 2009; Londoño et al. 2012) is adopted. The method involving dividing the structure into multiple substructures (Przemieniecki 1968) was developed to reduce the computational cost. The concept of substructuring can also be used to formulate a model wherein one (or more) part of the structure is a physical test specimen called the hardware in loop. In this case, the emulated structure combines experiment and theory. The theoretical substructure is the Software in the loop. This type of combined modelling is mainly suitable for structures wherein critical design element within the system can be identified. Critical elements generally have unpredictable or nonlinear behaviour. In the real time dynamic substructure implementation, the physical and numerical model is interfaced using actuators and sensors. The main source of

vibration would be the cutting action in the cutter shaft. The cutter shaft assembly is modeled as a software in the loop (SIL). The dredge hull with spud subjected to wave loading is modelled as a hardware in the loop (HIL). The interaction of the hull and spud is a complex phenomena. Therefore, this is modelled as the hardware in the loop. Induced forces acting on the cutter head are transmitted to the ladder support from the cutter head to the vessel deck. The current work focuses on the vibration transmission of the soil-spud-hull combined system to the dredge cutter shaft system subjected to wave loading. For the fatigue life, it is crucial to understand the vibration transmission on the cutter shaft when it is subjected to dynamic loading. Therefore, fatigue analysis of the cutter shaft is carried out for various conditions of the universal joint coupling.

2 System description

Modelling the effects of various system parameters on the vibration of the cutter suction dredger is carried out using a hybrid approach. The dredger hull assembly is analyzed as two subsystems. The first subsystem consists of the spud embedded in the soil and attached to the hull. This subsystem is modelled experimentally, forming the Hardware in the loop (HIL) (Bayati et al. 2013; Giberti and Ferrari 2015). The second subsystem is the cutter shaft assembly which is modelled theoretically, forming the Software in the loop (SIL). The purpose of choosing SIL for the cutter shaft subsystem is to explore a wider design parameter space. The coupled analysis of these subsystems (HIL and SIL) represents the hybrid modelling. The soil-spud-hull assembly is experimentally analyzed at the in-house towing tank facility at the Indian Institute of Technology Kharagpur. The cutter suction dredger (CSD) system is developed using a geometric scaling factor of 1:4, considering the constraint imposed by the towing tank dimensions.

2.1 Hardware in the loop subsystem

The HIL consists of the spud, soil embedment and dredge hull. The hull is attached with two spuds provided at the bow of the vessel. The central spud is the working spud, and the spud away from the centerline of the hull is the auxiliary spud. The auxiliary spud is active during the shifting of the cutting location. The basic layout and model scale dimensions of the hull are shown in Fig. 2.

Dynamic scaling of the system is carried out using a mixed approach by considering both Froude and Cauchy scaling for the system. The Froude scaling is adopted for the dredge hull and the Cauchy scaling is adopted for the cutter shaft system. The approach is adopted considering manufacturing and
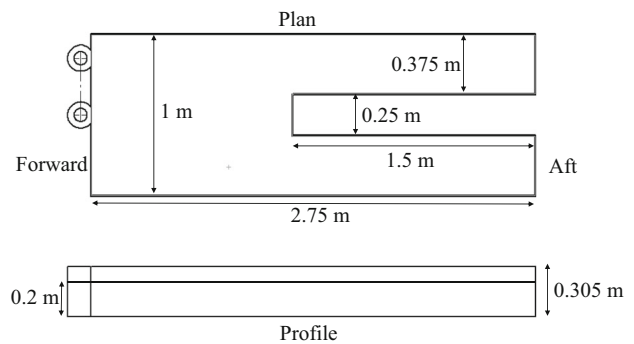

Fig. 2 Geometry of dredge hull

Fig. 3 Fabricated dredge hull model

Table 1 Material properties and hull dimensions

Parameter	Value
Length of hull	2.75 m
Beam of hull	1 m
Depth of hull	0.305 m
Draft of hull	0.2 m
Material of hull	Acrylic
Hull groove length	1.5 m
Hull groove width	0.25 m

Table 2 Spud material and dimension

Parameter	Value
Height of the spud	2.5 m
Outer diameter of the spud	0.083 m
Inner diameter of the spud	0.069 m
Spud length inside the soil	0.5 m
Spud material	Composite of aluminium and PVC

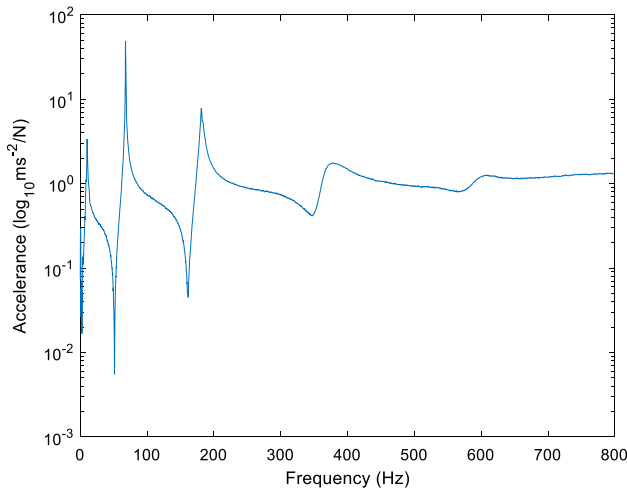**Fig. 4** Spud fabricated using PVC and Aluminium placed in the free-free condition

Fig. 5 Experimental frequency response function of the Spud in the free-free boundary condition
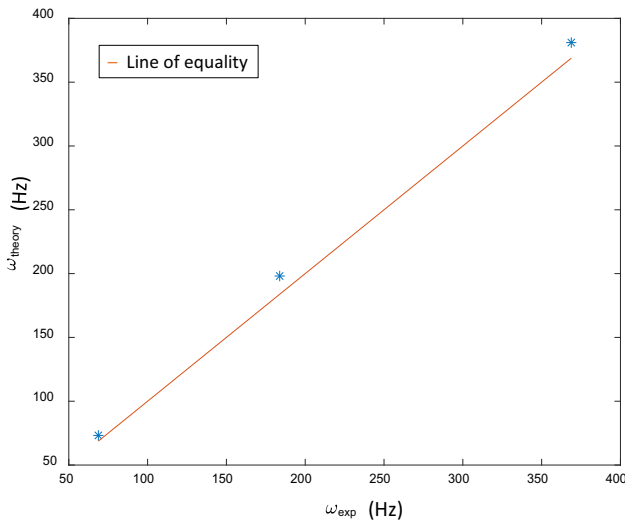

Fig. 6 Comparison of Experimental and theoretical natural frequency of the spud along with the line of equality

cost-effectiveness, and there is no loss of accuracy in the system characteristics. It is assumed that the dredge hull mainly undergoes rigid body motion with negligible flexural motion. When subjected to external waves, the dredge hull undergoes rigid body motion in the six degrees of freedom. Therefore, Froude scaling is adopted in modelling the dredge hull, considering the hull dimensions are a reasonable approximation. The dredge hull model is shown in Fig. 3. A raised forecastle is provided on the main deck of the dredge hull to restrict

green water loading during the experimental operation. The dredge hull model is made of Acrylic and a forecastle of plywood. The hull particulars are provided in Table 1. The hull is stiffened using Aluminium frames for sufficient strength. The weight of the bare hull is 197 kg. Ballast weights are added to the hull to attain the design draft displacement of 475 kg. The ballast weights are added to emulate the model scale longitudinal center of gravity (LCG), vertical center of gravity (VCG) and the pitch radius of gyration (Biran and López-Pulido 2014).

During the operational condition, only the working spud anchors into the soil and the auxiliary spud are kept idle. Therefore, the working spud is only considered for investigation in the present model. The spud connected to the dredge hull restrains the motion of the dredge hull. The dynamic forces on the spud are scaled, assuming that the spud undergoes flexural motion. The spud of the CSD system is modelled and designed using the same geometric scaling as the dredge hull. For selecting the spud material, Cauchy scaling criteria are considered assuming that the spud undergoes flexural motion. According to Cauchy scaling criteria, the relation between the model and prototype is given by:

$$\left(\frac{My}{EI}\right)_p = \left(\frac{My}{EI}\right)_m \tag{1}$$

where M = Bending moment, y = Distance to the outer surface from neutral axis and EI = Flexural rigidity

Accordingly, Young's modulus scales as:

$$E_p = \lambda E_m \tag{2}$$

where E_p = Elastic modulus of prototype, E_m = Elastic modulus of model and λ = Geometric scaling Ratio

The working spud is designed to maintain the scaled modulus of elasticity of the spud system. The elastic modulus of the prototype and model are 190 GPa and 47.5 GPa, respectively. The equivalent material is designed by the rule of mixture using Aluminium and PVC. According to the rule of mixtures, the density and Young's modulus of the composite system are estimated using:

$$\rho_m = \rho_p V_p + \rho_a V_a \tag{3}$$

$$E_{mt} = (E_p E_a) / (V_p E_a + V_a E_p) \tag{4}$$

where ρ_m = density of whole model, ρ_p = density of PVC, ρ_a = density of Aluminium, V_p = volume fraction of PVC, V_a = volume fraction of Aluminium, E_{mt} = elastic modulus in the transverse direction, E_p = elastic modulus of PVC, E_a = elastic modulus of Aluminium.

The spud dimensions and material are provided in Table 2. The hollow PVC pipe is bonded to a hollow Aluminium pipe. Due to the bonding, there could be a slight difference in the material properties. The actual Young's modulus of the fabricated model is determined by updating the theoretical model using Modal testing. Modal testing is carried out on the fabricated model in free-free boundary conditions, as shown in Fig. 4. An impulse hammer test is carried out where the hammer is impacted on the spud at a location given in Fig. 4. The response is measured using an accelerometer at the location given in Fig. 4. The resultant frequency response function obtained is shown in Fig. 5. The peaks in the FRF plots correspond to the natural frequencies of the spud.

Using a heuristic approach, the theoretical natural frequency of the spud is obtained using ANSYS. The modulus of elasticity of the spud is varied to reduce the error between the experimental and theoretical natural frequencies. After minimizing the error between the experimental and theoretical natural frequency, the equivalent Young's modulus of the spud is obtained as 45.7 GPa. A comparison of natural frequencies between experimental and theoretical is shown in Fig. 6.

2.2 Soil-spud and dredge hull assembly

The spud is placed in a cylindrical enclosure at an embedment depth of 0.5 m. The soil embedment is fixed on the towing tank base using a framed structure. Attachment of the framed structure to the dredge hull alters the mass distribution and, hence, the radius of gyration in the pitch. However, for the current study, the variation is considered less significant to influence the wave loading or the Hull response. To reduce the effective frame weight, buoyancy elements of foam are added in the hollow I-sections of the frame. The axial motion of the spud is restrained using a through bolt on the cylindrical embedment. The spud is connected to the dredge hull using a V-frame. The spud is located at different locations along the length of the V-frame using a movable collar/sleeve arrangement, as shown in Fig. 7. The collar forms a clearance fit with the spud, and the clearance is lubricated to allow free relative movement between the hull and the spud. The purpose of choosing such a clearance fit is also to emulate an impulsive loading from the dredge hull, which could occur during the dredging operation while pumping mud or debris. The impulsive loading can excite the different modes of the spud. The next step is to model the cutter shaft section of the system.

2.3 Software in the loop

The cutter shaft of the CSD, which forms the Software in the loop, is theoretically modelled using finite element analysis (Paz and Leigh 2004). The cutter shaft consists of two shafts coupled using the universal joint. The primary shaft does the cutting action, and the one connected to the dredge hull is called the secondary shaft. The primary and secondary shaft is modelled as an Euler–Bernoulli beam with five degrees of freedom per node, as shown in Fig. 8.

Corresponding elemental inertia and restoring force terms are.

$$F_{Inertia} = [\mathbf{M_{element}}]\ddot{X} = \frac{\rho A L}{420} \begin{bmatrix} 156 & 0 & 0 & 0 & 22L & 54 & 0 & 0 & 0 & -13L \\ 0 & 156 & 0 & -22L & 0 & 0 & 54 & 0 & 13L & 0 \\ 0 & 0 & 140J/A & 0 & 0 & 0 & 0 & -70J/A & 0 & 0 \\ 0 & -22L & 0 & 4L^2 & 0 & 0 & -13L & 0 & -3L^2 & 0 \\ 22L & 0 & 0 & 0 & 4L^2 & 13L & 0 & 0 & 0 & -3L^2 \\ 54 & 0 & 0 & 0 & 13L & 156 & 0 & 0 & 0 & -22L \\ 0 & 54 & 0 & -13L & 0 & 0 & 156 & 0 & 22L & 0 \\ 0 & 0 & -70J/A & 0 & 0 & 0 & 0 & 140J/A & 0 & 0 \\ 0 & 13L & 0 & -3L^2 & 0 & 0 & 22L & 0 & 4L^2 & 0 \\ -13L & 0 & 0 & 0 & -3L^2 & -22L & 0 & 0 & 0 & 4L^2 \end{bmatrix} \begin{bmatrix} \ddot{y}_1 \\ \ddot{z}_1 \\ \ddot{\theta}_{x_1} \\ \ddot{\theta}_{y_1} \\ \ddot{\theta}_{z_1} \\ \ddot{y}_2 \\ \ddot{z}_2 \\ \ddot{\theta}_{x_2} \\ \ddot{\theta}_{y_2} \\ \ddot{\theta}_{z_2} \end{bmatrix}$$

(5)

Fig. 7 Details of dredge hull-spud connection and the spud embedment
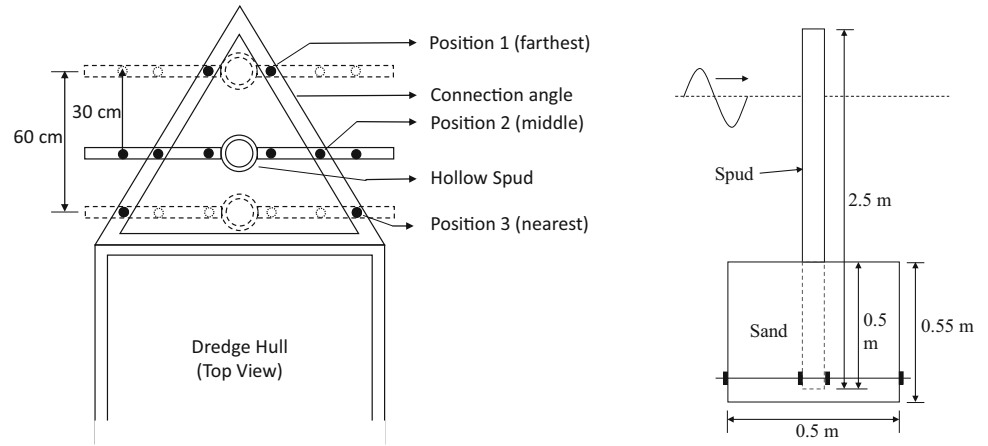
$$F_{Restoring} = [\mathbf{K_{element}}]X = \begin{bmatrix} 12EI/L^3 & 0 & 0 & 0 & 6EI/L^2 & -12EI/L^3 & 0 & 0 & 0 & 6EI/L^2 \\ 0 & 12EI/L^3 & 0 & -6EI/L^2 & 0 & 0 & -12EI/L^3 & 0 & -6EI/L^2 & 0 \\ 0 & 0 & GJ/L & 0 & 0 & 0 & 0 & -GJ/L & 0 & 0 \\ 0 & -6EI/L^2 & 0 & 4EI/L & 0 & 0 & 6EI/L^2 & 0 & 2EI/L & 0 \\ 6EI/L^2 & 0 & 0 & 0 & 4EI/L & -6EI/L^2 & 0 & 0 & 0 & 2EI/L \\ -12EI/L^3 & 0 & 0 & 0 & -6EI/L^2 & 12EI/L^3 & 0 & 0 & 0 & -6EI/L^2 \\ 0 & -12EI/L^3 & 0 & 6EI/L^2 & 0 & 0 & 12EI/L^3 & 0 & 6EI/L^2 & 0 \\ 0 & 0 & -GJ/L & 0 & 0 & 0 & 0 & GJ/L & 0 & 0 \\ 0 & -6EI/L^2 & 0 & 2EI/L & 0 & 0 & 6EI/L^2 & 0 & 4EI/L & 0 \\ 6EI/L^2 & 0 & 0 & 0 & 2EI/L & -6EI/L^2 & 0 & 0 & 0 & 4EI/L \end{bmatrix} \begin{bmatrix} y_1 \\ z_1 \\ \theta_{x1} \\ \theta_{y1} \\ \theta_{z1} \\ y_2 \\ z_2 \\ \theta_{x2} \\ \theta_{y2} \\ \theta_{z2} \end{bmatrix} \quad (6)$$

where ρ is the density of the element, A is the area of the element, L is the length of the element, E is the Elastic modulus of the element, I is the moment of inertia of the element, G is the Shear modulus of the element, and J is the polar moment of inertia of the element. The universal joint is modelled as a discrete spring element. The structural damping is considered as Proportional Rayleigh damping with α and β as 0.01 and 0.0002, respectively. The forces acting on the cutter shaft system due to wave loading are estimated using the Morison equation (Sarpkaya 2010). The effect of relative velocity between the wave and structure is neglected. The wave force is given by:

$$F(t) = \frac{1}{2}\rho C_d D L U|U| + \rho C_m A L \dot{U} \quad (7)$$

where, based on the linear wave theory water particle acceleration is obtained as

$$\dot{U} = agk \frac{\cosh k(H+z)}{\cosh kH} sin(kx - \omega t) \quad (8)$$

and water particle velocity is obtained as

$$U = \frac{agk}{\omega} \frac{\cosh k(H+z)}{\cosh kH} \cos(kx - \omega t) \quad (9)$$

where C_m is the inertia coefficient, C_d is the drag coefficient, ρ is the density of water, A is the projected area of the cutter shaft, D is the diameter of the cutter shaft, L is the length of the cutter shaft, k is the wave number, H is the depth of water, z is the specific depth below the free surface of the water, and a is the wave amplitude.

3 Experimental analysis of the HIL

A dynamic analysis is carried out for the dredge hull and dredge hull-spud assembly using a back paddle-type DHI wave maker. The dredge hull spud assembly with different positions of the spud is shown in Fig. 9. The wave input is provided using DHI wave synthesizer, and the wave generated is measured using two wave probes located upstream and downstream of the dredge hull. Generated waves require a minimum 15 m (two-wavelength) from the paddle of the wave maker to achieve fully developed conditions; therefore,
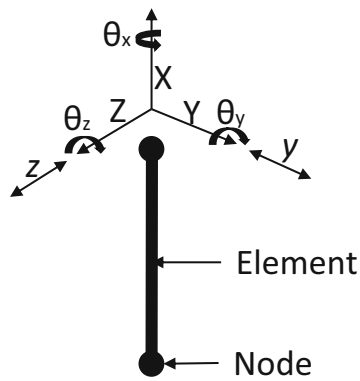
Fig. 8 Two-Noded element with five DOF

the upstream wave probe is fitted 18 m away from the paddle of the wave maker. The dredge hull model is subjected to a linear sinusoidal wave of height 10 cm with periods ranging from 0.67 to 2.5 s under head sea conditions for 90 s.

The temporal response of the hull subjected to wave loading is recorded using Motion Reference Unit (MRU) (2019), which is attached at an accessible location within the hull. The center of gravity (CG) of the dredge hull is determined using a swing test (Hinrichsen 1991; Onas and Datla 2009). Since the MRU is located offset from the CG, the response

is transformed to CG using an in-built Kalman filter within the unit. An accelerometer is connected at the top of the free end of the spud to record the temporal response of the soil-spud-hull assembly using the OROS (2020) data acquisition system.

When subjected to external waves, the dredge hull exhibits rigid body motion in six degrees of freedom. It is observed that due to wave loading heave and pitch motions are relatively higher compared to other rigid body modes of the Hull. The spud restraints motion of the hull in the vertical plane and acts as a pivot point. Therefore, among the rigid body modes of the hull heave and pitch is the one which is most restrained by the spud. Therefore, the response amplitude operators (RAO) of only these two motions are considered and analyzed for the complete investigation of the system. RAO is the heave and pitch response ratio to the wave height and wave slope, respectively. The natural frequency of the heave and pitch motions are evaluated for the dredge hull. The experimental results are compared with those obtained from MAXSURF (2013, 2014) using Panel Method. MAXSURF motion module analyses the dredge hull response assuming the potential flow solving the first order radiation diffraction problem using constant panel-based boundary element method (BEM). The heave and pitch natural frequencies
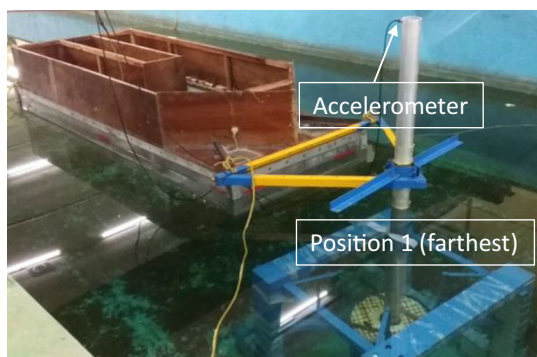
(a) Position 1 of the spud
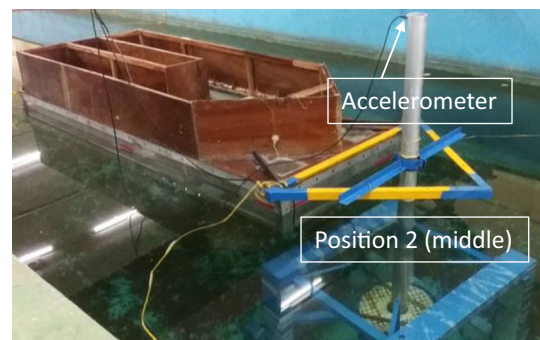
(b) Position 2 of the spud
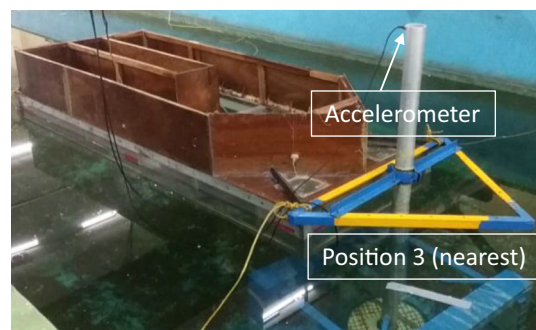
(c) Position 3 of the spud

Fig. 9 Dredge hull-spud assembly of different spud locations subjected to wave loading in the towing tank
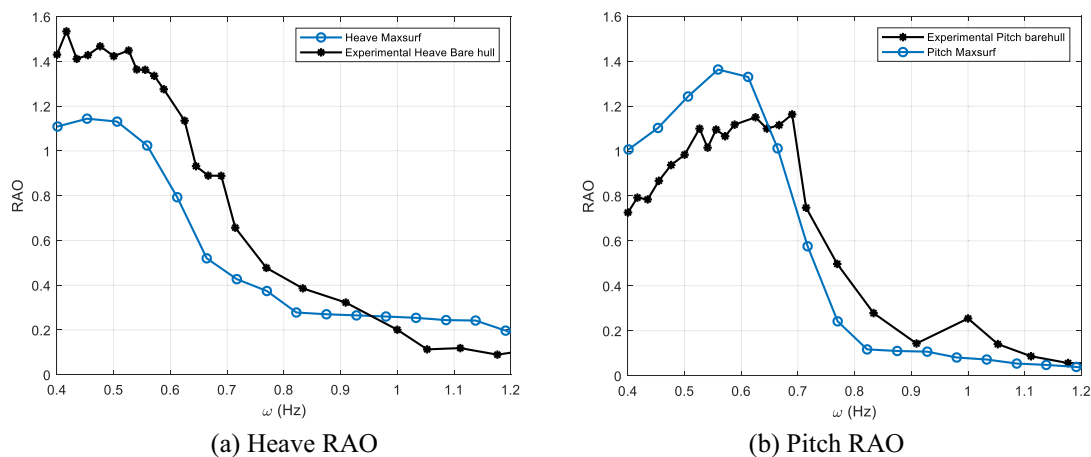
(a) Heave RAO

(b) Pitch RAO

Fig. 10 Experimental and numerical comparison of the hull for different wave excitation frequencies under head sea condition

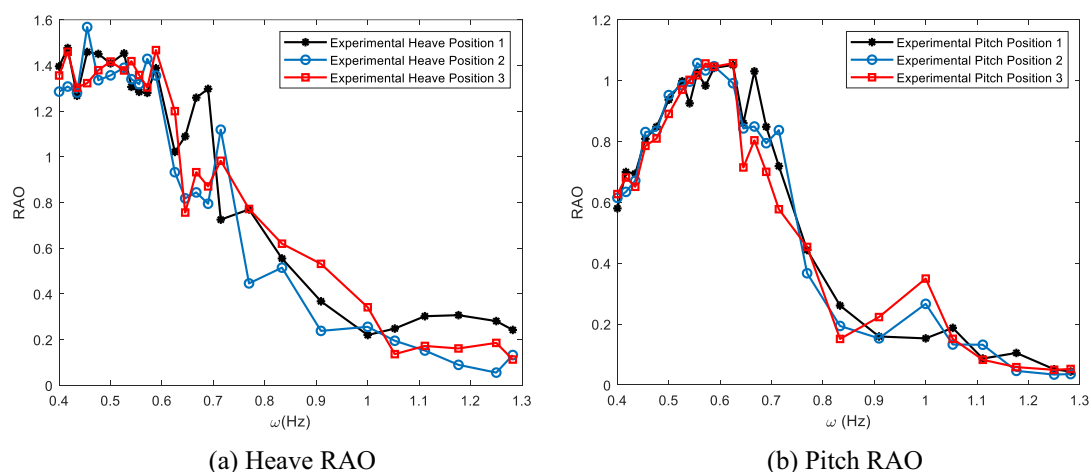(a) Heave RAO

(b) Pitch RAO

Fig. 11 Experimental comparison of the hull for different spud locations and wave excitation frequency under head sea condition

comparisons are shown in Fig. 10. The slight difference in heave and pitch natural frequencies and magnitude could be due to approximations in the numerical modelling the groove in the hull provided for the spud. Also, a restraint is provided to the hull to avoid drifting of the hull using a rope which is not considered in the numerical model. Next, the variability in the hull response with change in the effectiveness of the restraint imposed by the spud is analyzed.

The response of the dredge hull by varying the position of the spud relative to the dredge hull is analyzed. The dredge hull-spud system is subjected to regular waves for the same wave parameter as the bare dredge hull. The variation in heave and pitch Response amplitude operator (RAO) shown in Fig. 11 indicates that the presence of spud reduces the pitch RAO, and there is a slight shift in the heave and pitch frequencies.

4 Coupling the hybrid system

From the previous theoretical study (Vijayan et al. 2021) carried out on the vibration transmission of the cutter shaft, it was observed that the maximum acceleration amplification (Vijayan 2012; Vijayan and Woodhouse 2013, 2014) occurs for the same length between the primary and secondary shaft. Therefore, for further analysis of the system, the relative lengths of the two shafts of the cutter shaft system are kept the same to represent the maximum vibration transmission.

In the practical scenario, coupling between HIL and SIL is bound to have issues due to delay in the response from the numerically emulated system (Wallace 2006). Assuming the SIL to be an SDOF system which in the system is assumed to the lowest natural frequency of the SIL system.
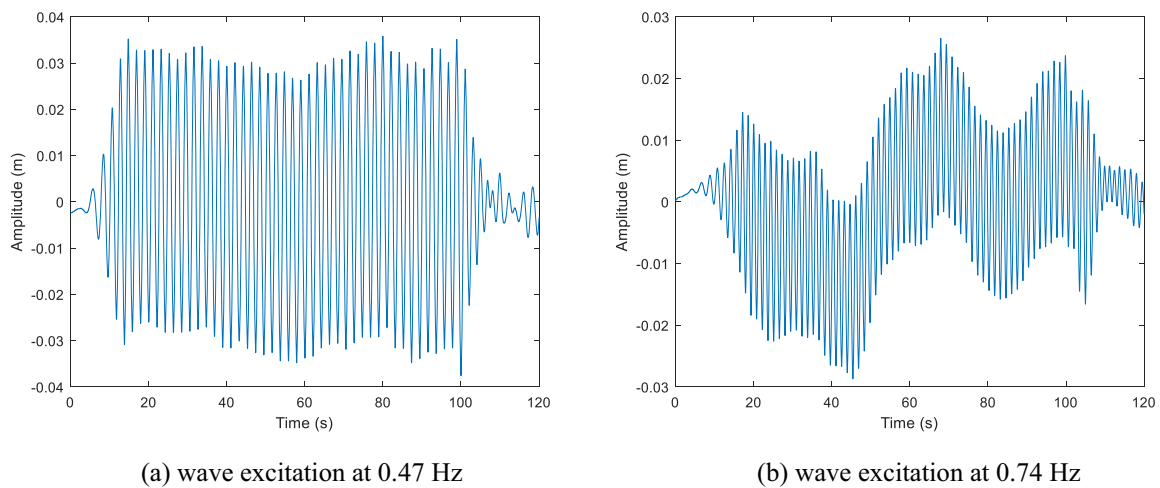
(a) wave excitation at 0.47 Hz

(b) wave excitation at 0.74 Hz

Fig. 12 Time response of hull with spud at different wave excitation frequencies

The state of the system is represented by z_{em}, which indicates the dynamics of the emulated system. A substructured model of the system is created by isolating the spring k_{act} to represent the actuator dynamics. The resultant equation of motion is given as

$$m\ddot{z} + c\dot{z} + kz = F \qquad (10)$$

where the feedback force F is the substructure response given $F = -k_{act}y$ with $y = z(t - \tau)$.

The actuator system cannot react instantaneously to the change of state of the numerical model and thus induces a delay in the response. Thus the equation of motion reduces to

$$m\ddot{z} + c\dot{z} + kz + k_{act}z(t - \tau) = 0 \qquad (11)$$

The equation of motion is given by

$$m\ddot{z} + c\dot{z} + kz + k_{act}y = 0 \qquad (12)$$

which reduces to

$$\ddot{z} + 2\xi\beta\dot{z} + \omega_n^2 z + \alpha y = 0 \qquad (13)$$

where ξ is the damping ratio, and ω_n is the natural frequency, $\alpha = \frac{k_{act}}{m}$ and $\beta = \omega/\omega_n$.

Assuming the solution of the form $z = Ae^{\lambda t}$ we obtain

$$\lambda^2 + 2\xi\beta\lambda + \omega_n^2 + \alpha e^{-\lambda\tau} = 0 \qquad (14)$$

Assuming delay τ to be small, we can approximate $e^{-\lambda\tau} \simeq 1 - \lambda\tau$. Eq. reduces to:

$$\lambda^2 + 2\xi\beta\lambda + \omega_n^2 + \alpha(1 - \lambda\tau) = 0 \qquad (15)$$

The roots of the equation are given by:

$$\lambda_{1,2} = \frac{-(2\xi\beta - \alpha\tau) \pm \sqrt{(2\xi\beta - \alpha\tau)^2 - 4(\omega_n^2 + \alpha)}}{2} \qquad (16)$$

The system stability is determined by the real part of the root. The change in damping from a positive to a negative value based on the delay as a bifurcation parameter can lead to sustained oscillations. This results in hopf bifurcation. The stability criteria are obtained as:

$$\alpha\tau < 2\xi\beta \Rightarrow \tau_c < \frac{2\xi\beta}{\alpha} \qquad (17)$$

The delay can be compensated using a feed-forward controller. The feed-forward controller predicts the actuator response based on the SIL response and compensates for the delay induced in the system. Since the prediction calculation time needs to be small, this can be complemented using a nth order polynomial function based on the present and n previous calculated values given by

$$x' = \sum_{i=0}^{n} a_i x_i \qquad (18)$$

where n is the order of prediction, x_0 is the present calculated displacement, x_i is the calculated displacement $\delta + x_i$ unit time ago, and a_i is the constants.
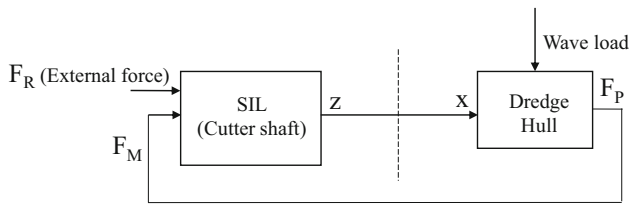
Fig. 13 Flowchart of the system analysis coupling Hardware in the loop and Software in the loop

Order n	a_0	a_1	a_2	a_3	a_n
0	1	–	–	–	–
1	2	-1	–	–	–
2	3	-3	1	–	–
3	4	-6	4	-1	–
4	5	-10	10	-5	1

In the current study, HIL is not tested in real time using embedded SIL system. The process flowchart is shown in Fig. 13. It is assumed that the desired response from the numerical model is the same as the actuator response, i.e. $z = x$. Therefore, in the current study controller is not designed which is used to accommodate the actuator delay. Similarly, in the measured response, the sensor dynamics are not considered, i.e., $F_p = F_M$. System identification is carried out on the HIL using the accelerometer response. The purpose of using an accelerometer for identifying the system is to include the frequency response of the spud. The typical temporal response of the dredge hull with spud at two different wave excitation, namely 0.47 Hz and 0.74 Hz, is shown in Fig. 12. At 0.74 Hz, both heave and pitch motions are coupled as indicated by the temporal response. Therefore, for further analysis, this frequency of excitation is chosen (Fig. 12, 13).

To pass the dynamic parameters across the HIL and SIL, a system identification on the HIL system is carried out. The system is identified using the System identification toolbox in MATLAB. The identified forced SDOF in the lateral direction is coupled to the lateral DOF of the cutter shaft, as shown in Fig. 14.

System identification is carried out for three different configurations of the spud relative to the hull. The equation of motion of the system is transformed into the state space. The equation of motion of the system is given by:

$$[(\mathbf{M} + \mathbf{M_a})_{\mathbf{SIL}} + \mathbf{M_{HIL}}]\ddot{x}(t) + [C]\dot{x}(t) + [K_{\mathbf{SIL}} + \mathbf{K_{HIL}}]\mathbf{x(t)} = \mathbf{F} \quad (19)$$

where $\mathbf{M}$ is the global mass matrix of the cutter shaft system, $\mathbf{M_a}$ is the added mass of the cutter shaft system, $\mathbf{K_{SIL}}$ is the global stiffness matrix of the cutter shaft system, $\mathbf{M_{HIL}}$

and $\mathbf{K_{HIL}}$ are the mass and stiffness of SDOF identified HIL system, $\mathbf{C}$ is the proportional Rayleigh damping using α and β values 0.01 and 0.0002, respectively, and $\mathbf{F}$ is the force vector of the system.

Furthermore, the state-space transformed equation is:

$$\begin{bmatrix} \dot{\mathbf{x}} \\ \ddot{\mathbf{x}} \end{bmatrix} = \begin{bmatrix} \mathbf{0} & \mathbf{I} \\ -\mathbf{K_{Hybrid}}/\mathbf{M_{Hybrid}} & -\mathbf{C}/\mathbf{M_{Hybrid}} \end{bmatrix} \begin{bmatrix} \mathbf{x} \\ \dot{\mathbf{x}} \end{bmatrix} + \begin{bmatrix} \mathbf{0} \\ \mathbf{F}/\mathbf{M_{Hybrid}} \end{bmatrix} \quad (20)$$

where

$$\begin{bmatrix} \mathbf{M_{Hybrid}} \end{bmatrix} = \begin{bmatrix} (\mathbf{M} + \mathbf{M_a})_{\mathbf{SIL}} + \mathbf{M_{HIL}} \end{bmatrix} \quad (21)$$

$$\begin{bmatrix} \mathbf{K_{Hybrid}} \end{bmatrix} = [\mathbf{K_{SIL}} + \mathbf{K_{HIL}}] \quad (22)$$

The system is subjected to a transient loading using an initial velocity in the lateral and torsional direction with a bandwidth of 500 Hz. The universal joint is modelled using coupling springs of high and low stiffness. The maximum acceleration obtained along the cutter shaft is determined. An acceleration ratio is determined by taking the ratio of maximum acceleration corresponding to low coupling to the high coupling stiffness. The coupling strength of the universal joint is varied, and the maximum acceleration observed across the cutter shaft assembly is noted (Vijayan et al. 2021). Acceleration amplification for the three different configurations is determined, and the results shown in Fig. 15 indicate that the acceleration amplification is less sensitive to the spud position.

The results from the acceleration amplification study indicate that high coupling strength reduces the acceleration amplification for the same length ratio between the primary and secondary shaft. Since the cutting action and wave loading cause periodic loading on the cutter shaft, whether the design is better for fatigue life needs to be verified.

4.1 Fatigue analysis

The fatigue response of the cutter shaft is analyzed by simulating the response for 10 min. Periodic wave excitation is provided at the same frequency for which the HIL system is identified. The variation in wave force along the length of the cutter shaft is determined using the Morison equation. A periodic force of 15 N at 0.5 radians/s corresponding to the prototype periodic force of 1 kN at 1 rad/s is provided to emulate the cutting action. Assuming five blades each is exciting the cutter shaft at a phase difference of 36 degrees. The cutter excitation is provided at the last node in the lateral DOF along the wave excitation direction. This assumption is valid for a continuous cutting action; however, in reality,
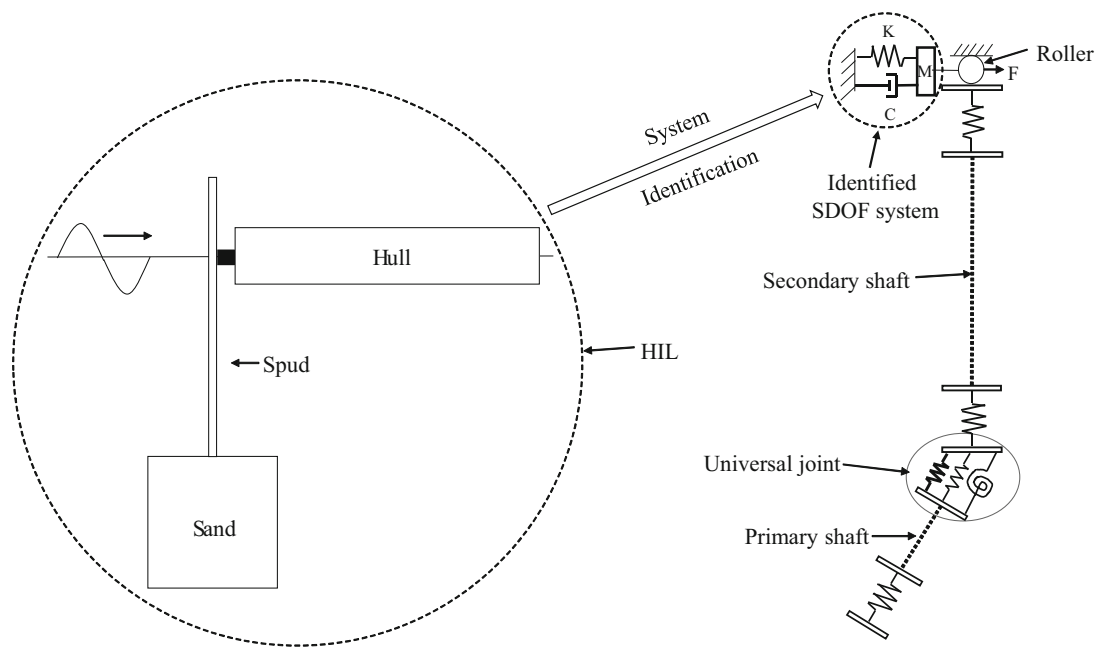
Fig. 14 Schematic of the equivalent SDOF of the HIL coupled to the cutter shaft assembly (SIL)
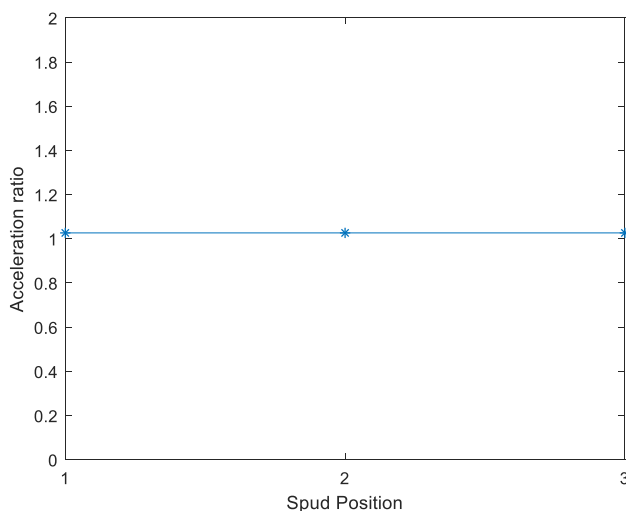

Fig. 15 Variation of acceleration ratio for different positions of the connectivity between spud and hull

this could be discontinuous and requires a delay differential equation (Balachandran 2001) to solve the system. The displacement response and the stiffness of the cutter shaft give the forces exerted on the cutter shaft system. These forces upon the projected area of the cutter shaft lead to generate stress on the cutter shaft system. The rainflow cycle counting is performed in MATLAB by considering the 10-min stress time history of the cutter shaft system. Two positions are critical in the cutter shaft system to analyze the fatigue, i.e., (a) the bottom of the primary shaft at the cutting location and (b) the location of the universal joint. The current

study location of the universal joint is analyzed for fatigue life. The rainflow matrix obtained in each cycle contributes to a certain amount of fatigue damage. The universal joint controls the vibration transmission from the primary shaft to the secondary shaft. The previous study (Vijayan et al. 2021) indicated that a high coupling strength reduces acceleration amplification. The rainflow matrices for the low universal joint coupling strength of the universal joint of different parts of the cutter shaft system are shown in Fig. 16, and Fig. 18, and the rain-flow matrices with high universal joint coupling strength are shown in Fig. 17 and Fig. 19. The results from the rainflow counting indicate a high-stress cycle level observed for high coupling strength. Therefore, even though high coupling strength reduces the acceleration amplification, it need not result in good fatigue life (Fig. 16, 17, 18, 19).

5 Conclusions

The critical design consideration for a cutter suction dredger is analyzed using a hybrid approach of HIL and SIL. From the experimental analysis carried out on the HIL system consisting of dredge hull and spud, the system frequency response of the heave and pitch response is determined. To model the dredge hull and spud, a geometric scaling of 1:4 is considered. For dynamic scaling, it is assumed that the dredge hull is mainly subjected to rigid body motion and the spud embedded in the soil is subjected to flexural loading. Therefore, the dredge hull fabricated using Acrylic and Aluminium frames is scaled following Froude scaling. Spud is designed as a
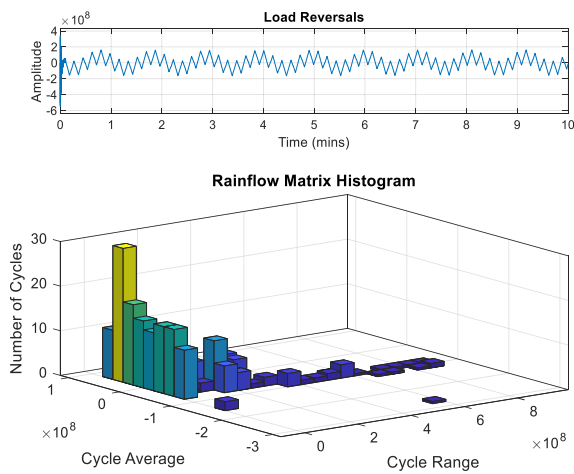
Fig. 16 Rain flow matrix of cutter end of the primary shaft with low coupling strength of the universal joint
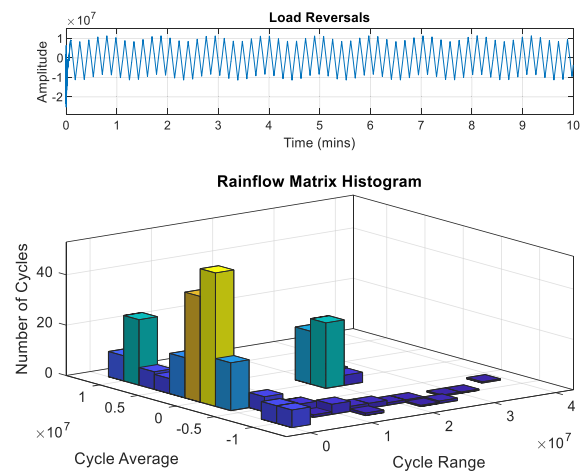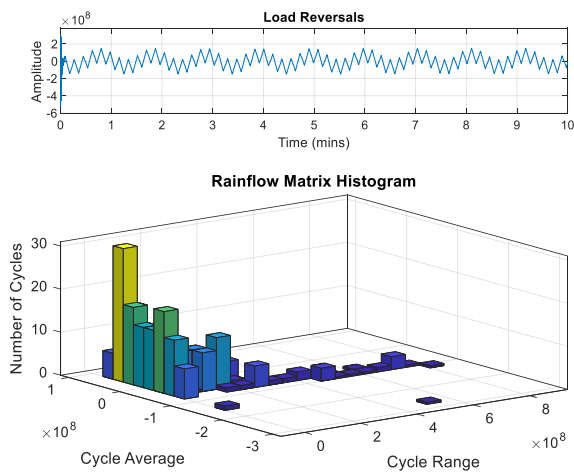

Fig. 17 Rain flow matrix of cutter end of the primary shaft with high coupling strength of the universal joint
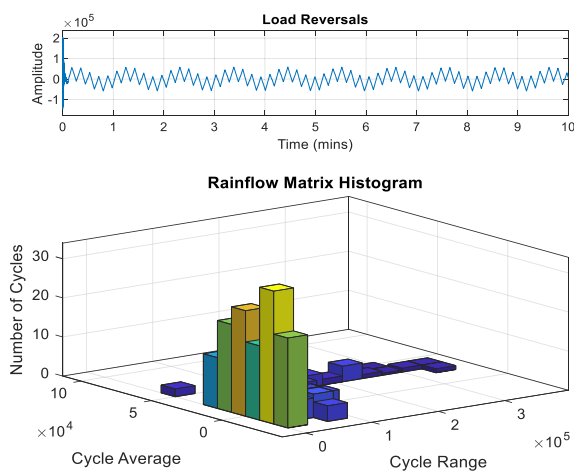

Fig. 18 Rain flow matrix at the universal joint position of cutter shaft system with low coupling strength of the universal joint

Fig. 19 Rain flow matrix at the universal joint position of cutter shaft system with high coupling strength of the universal joint

composite cylinder of Aluminium and PVC using the rule of mixture. The equivalent spud satisfies the Cauchy scaling with reasonable accuracy confirmed using modal testing on the structure. The dredge hull is analyzed in MAXSURF motion and compared with the experimental pitch and heave RAOs. The analysis of the spud attached to the dredge hull indicates that the RAO reduces with the attachment of the spud. System identification is carried out on the HIL system for three different positions of the spud relative to the hull. The HIL system is identified as an SDOF in the lateral direction coupled to the SIL. Analysis of the hybrid system comprising HIL and SIL is carried out in state space by coupling the lateral DOF of the identified HIL and lateral DOF of the FEM model of the SIL cutter shaft. Based on the previous studies on acceleration amplification in coupled structures (Vijayan et al. 2021), a high coupling stiffness causes less acceleration amplification along the cutter shaft. A sensitive analysis of the acceleration amplification based on the relative spud location is carried out. The results from the sensitivity analysis indicate that the acceleration amplification is insensitive to the spud location relative to the hull. Next, a fatigue analysis is carried out on the hybrid system by simulating the response for 10 min. The system is subjected to wave and periodic loading due to cutting action. Based on the fatigue analysis carried out using rainflow counting, it is observed that the stress cycle levels are higher for high coupling stiffness. Hence even though a high coupling reduces acceleration amplification, it can reduce the fatigue life of the cutter shaft. Therefore, at the design phase of the cutter shaft, the coupling of the universal joint should be designed optimally to satisfy moderate acceleration amplification, shaft length and fatigue loading.

Declarations

Conflict of interest The authors declare that they have no known competing financial interests or personal relationships that could have appeared to influence the work reported in this paper.

References

Amzallag C, Gerey J, Robert J, Bahuaud J (1994) Standardization of the rainflow counting method for fatigue analysis. Int J Fatigue 16:287–293. https://doi.org/10.1016/0142-1123(94)90343-3

Arena F, Nava V (2008) On linearization of Morison force given by high three-dimensional sea wave groups. Probab Eng Mech 23:104–113. https://doi.org/10.1016/j.probengmech.2007.12.010

Ariduru S (2004) Fatigue life calculation by rainflow cycle counting method. MS Master of Science,Mechanical Engineering, Middle East Technical University

Baek SH, Cho SS, Joo WS (2008) Fatigue life prediction based on the rainflow cycle counting method for the end beam of a freight car bogie. Int J Automot Technol 9:95–101. https://doi.org/10.1007/s12239-008-0012-y

Balachandran B (2001) Nonlinear dynamics of milling processes. Philos Trans R Soc Lond Ser A Math Phys Eng Sci 359:793–819. https://doi.org/10.1098/rsta.2000.0755

Bayati I, Belloli M, Facchinetti A, Giappino S (2013) Wind tunnel tests on floating offshore wind turbines: a proposal for hardware-in-the-loop approach to validate numerical codes. Wind Eng 37:557–568. https://doi.org/10.1260/0309-524X.37.6.557

Bentley Systems, US (2013) Maxsurf Motions Windows User Manual Version 20

Bentley Systems, US (2014) Maxsurf Modeler Windows User Manual Version 20

Biran AB, López-Pulido R (2014) Ship hydrostatics and stability, 2nd edn. Butterworth-Heinemann, Elsevier

Bursi OS, David W (2009) Modern testing techniques for structural systems: dynamics and control, vol 502. Springer Science & Business Media

Chaplin JR, Rainey RCT, Yemm RW (1997) Ringing of a vertical cylinder in waves. J Fluid Mech 350:119–147. https://doi.org/10.1017/S002211209700699X

Chen X, Miedema SA, van Rhee C (2014) Numerical Methods for modeling the rock cutting process in deep sea mining. Offshore geotechnics, vol 3. American Society of Mechanical Engineers

Chen X, Miedema SA, van Rhee C (2015) Numerical modeling of excavation process in dredging engineering. Procedia Eng 102:804–814. https://doi.org/10.1016/j.proeng.2015.01.194

de Koning J, Miedema SA, Zwartbol A (1983) Soil/cutterhead interaction under wave conditions. In: Proc. WODCON X, Singapore

Giberti H, Ferrari D (2015) A novel hardware-in-the-loop device for floating offshore wind turbines and sailing boats. Mech Mach Theory 85:82–105. https://doi.org/10.1016/J.MECHMACHTHEORY.2014.10.012

Glover GJ (2002) Laboratory modeling of hydraulic dredges and design of dredge carriage for laboratory facility. Master's Thesis, Ocean Engineering Program, Civil Engineering Department, Texas A&M University, College Station

Glover G, Randall R (2004) Scaling of model hydraulic dredges with application to design of a dredge modeling facility. J Dredg Eng West Dredg Assoc 6:15–35

Helmons RLJ, Miedema SA (2013) Rock cutting for deep sea mining: an extension into poromechanics. Poromechanics V. American Society of Civil Engineers, Reston, pp 2381–2390

Helmons RLJ, Miedema SA, van Rhee C (2014) A new approach to model hyperbaric rock cutting processes. Ocean space utilization Professor Emeritus J Randolph Paulling honoring symposium on ocean technology, vol 7. American Society of Mechanical Engineers

Hinrichsen P (1991) The measurement of weight distribution of olympic class dinghies and keelboats. In: 10th Chesapeake Sailing Yacht Symposium. Annapolis

Inertial Labs, US (2019) MRU GUI User's Manual Revision 1.5

Jameel M, Oyejobi DO, Siddiqui NA, Ramli Sulong NH (2017) Nonlinear dynamic response of tension leg platform under environmental loads. KSCE J Civ Eng 21:1022–1030. https://doi.org/10.1007/s12205-016-1240-8

Lagoda T (1996) Influence of correlations between stresses on calculated fatigue life of machine elements. Int J Fatigue 18:547–555. https://doi.org/10.1016/S0142-1123(96)00025-4

Londoño JM, Serino G, Wagg DJ et al (2012) On the assessment of passive devices for structural control via real-time dynamic substructuring. Struct Control Heal Monit 19:701–722. https://doi.org/10.1002/stc.464

Marsh G, Wignall C, Thies PR et al (2016) Review and application of Rainflow residue processing techniques for accurate fatigue damage estimation. Int J Fatigue 82:757–765. https://doi.org/10.1016/j.ijfatigue.2015.10.007

Miedema SA (2009) New developments of cutting theories with respect to dredging, the cutting of clay and rock. WEDA XXIX & Texas a&m 40:14–17

Miedema SA (1986) Underwater soil cutting: a study in continuity. Dredg Port Constr, pp 47–53

Miedema SA (1989) The cutting forces in saturated sand of a seagoing cutter suction dredger. In: Proc. WODCON XII, Orlando, Florida, USA. Orlando, Florida

Miedema SA (1992) New developments of cutting theories with respect to dredging, the cutting of clay. In: Proc. WODCON XIII. Bombay, India

Mockutė A, Marino E, Lugni C, Borri C (2017) Comparison of hydrodynamic loading models for vertical cylinders in nonlinear waves. Procedia Eng 199:3224–3229. https://doi.org/10.1016/j.proeng.2017.09.329

Najafian G, Tickell RG, Burrows R, Bishop JR (2000) The UK Christchurch Bay Compliant Cylinder Project: analysis and interpretation of Morison wave force and response data. Appl Ocean Res 22:129–153. https://doi.org/10.1016/S0141-1187(00)00009-2

Onas AS, Datla R (2009) Experimental analysis of roll damping of a trimaran with varying side hull stagger and transverse spacing. In: WMTC Conference. Stevens Institute of Technology, Hoboken

OROS (2020) OROS 3-Series/NVGate Reference Manual V12.00. Oros Gmbh

Paz M, Leigh W (2004) Structural dynamics: theory and computation, 5th edn. Springer + Business Media, New York

Plummer AR (2006) Model-in-the-loop testing. Proc Inst Mech Eng Part I J Syst Control Eng 220:183–199. https://doi.org/10.1243/09596518JSCE207

Prasad SR, Sekhar AS (2018) Life estimation of shafts using vibration based fatigue analysis. J Mech Sci Technol 32:4071–4078. https://doi.org/10.1007/s12206-018-0806-4

Przemieniecki JS (1968) Discrete-element methods for stability analysis of complex structures. Aeronaut J 72:1077–1086. https://doi.org/10.1017/s0001924000085778

Randall RE, Dejong P, Sonye S et al (2005) Laboratory dredge carriage for modeling dredge operations. In: Proceedings of the Western Dredging Association Twenty-fifth Technical Conference and Thirty-seventh Annual Texas A&M Dredging Seminar, College Station, TX, USA, pp 17–29

Rédl J (2018) Processing of stress dataset with rain-flow counting method. Math Educ Res Appl 4:9–17. https://doi.org/10.15414/meraa.2018.04.01.9-17

Salvinder S, Shahrum A, Mohamed NAN (2016) Discretized Markov chain in damage assessment using Rainflow cycle with effects of mean stress on an automobile crankshaft. J Mech Sci Technol 30:3539–3551. https://doi.org/10.1007/s12206-016-0714-4

Sarpkaya T (2010) Wave forces on offshore structures. Cambridge University Press, Cambridge

Sclavounos PD, Zhang Y, Ma Y, Larson DF (2019) Offshore wind turbine nonlinear wave loads and their statistics. J Offshore Mech Arct Eng 10(1115/1):4042264

Shen YP, Wang SL, Li XJ, Dhillon BS (2010) Multiaxial fatigue life prediction of kiln roller under axis line deflection. Appl Math Mech (english Ed) 31:205–214. https://doi.org/10.1007/s10483-010-0208-x

Soeb MR, Islam ABMS, Jumaat MZ et al (2017) Response of nonlinear offshore spar platform under wave and current. Ocean Eng 144:296–304. https://doi.org/10.1016/j.oceaneng.2017.07.042

Stansberg CT (1997) Comparing ringing loads from experiments with cylinders of different diameters—an empirical study. ETDEWEB, London

van Os AG, van Leussen W (1987) Basic research on cutting forces in saturated sand. J Geotech Eng 113:1501–1516. https://doi.org/10.1061/(ASCE)0733-9410(1987)113:12(1501)

Vijayan K (2012) Vibration and shock amplification of drilling tools. Doctoral dissertation. University of Cambridge, UK

Vijayan K, Woodhouse J (2013) Shock transmission in a coupled beam system. J Sound Vib 332:3681–3695. https://doi.org/10.1016/j.jsv.2013.02.024

Vijayan K, Woodhouse J (2014) Shock amplification, curve veering and the role of damping. J Sound Vib 333:1379–1389. https://doi.org/10.1016/j.jsv.2013.10.037

Vijayan K, Barik CR, Sha OP (2021) Shock transmission through universal joint of cutter suction dredger. Ocean Eng. https://doi.org/10.1016/j.oceaneng.2021.109185

Wagg DJ, Stoten DP (2001) Substructing of dynamical systems via the adaptive minimal control synthesis algorithm. Earthq Eng Struct Dyn 30:865–877. https://doi.org/10.1002/eqe.44

Wallace MI (2006) Real-time dynamic substructuring for mechanical and aerospace applications : control techniques and experimental methods. Doctoral dissertation, University of Bristol, UK

Wolfram J (1999) On alternative approaches to linearization and Morison's equation for wave forces. Proc R Soc Lond Ser A Math Phys Eng Sci 455:2957–2974. https://doi.org/10.1098/rspa.1999.0434

Wolfram J, Naghipour M (1999) On the estimation of Morison force coefficients and their predictive accuracy for very rough circular cylinders. Appl Ocean Res 21:311–328. https://doi.org/10.1016/S0141-1187(99)00018-8

Yasheng M, Fusheng N, Miedema SA (2006) Calculation of the blade cutting force for small cutting angles based on MATLAB. In: The 2nd China Dredging Association International Conference & Exhibition, Guangzhou, China

Yigang Z, Shijie Z, Minggao Y (1993) A cycle counting method considering load sequence. Int J Fatigue 15:407–411. https://doi.org/10.1016/0142-1123(93)90487-B

Young DR (2009) Forces on laboratory model dredge cutterhead. Master's Thesis. Texas A&M University, College Station